Combustion and Flame 158 (2011) 291–300

Contents lists available at ScienceDirect

Combustion and Flame

journal homepage: www.elsevier.com/locate/combustflame

On the extraction of laminar flame speed and Markstein length from outwardly propagating spherical flames

Zheng Chen

State Key Laboratory for Turbulence and Complex Systems, Department of Mechanics and Aerospace Engineering, College of Engineering, Peking University, Beijing 100871, China

ARTICLE INFO

Article history:
Received 26 April 2010
Received in revised form 6 June 2010
Accepted 1 September 2010

Keywords:
Extraction
Laminar flame speed
Markstein length
Propagating spherical flame

ABSTRACT

Large discrepancies among the laminar flame speeds and Markstein lengths of methane/air mixtures measured by different researchers using the same constant-pressure spherical flame method are observed. As an effort to reduce these discrepancies, one linear model (LM, the stretched flame speed changes linearly with the stretch rate) and two non-linear models (NM I and NM II, the stretched flame speed changes non-linearly with the stretch rate) for extracting the laminar flame speed and Markstein length from propagating spherical flames are investigated. The accuracy and performance of the LM, NM I, and NM II are found to strongly depend on the Lewis number. It is demonstrated that NM I is the most accurate for mixtures with large Lewis number (positive Markstein length) while NM II is the most accurate for mixtures with small Lewis number (negative Markstein length). Therefore, in order to get accurate laminar flame speed and Markstein length from spherical flame experiments, different non-linear models should be used for different mixtures. The validity of the theoretical results is further demonstrated by numerical and experimental studies. The results of this study can be used directly in spherical flame experiments measuring the laminar flame speed and Markstein length.

1. Introduction

The laminar flame speed is defined as the speed relative to the unburned gas, with which a planar, one-dimensional flame front travels along the normal to its surface [1]. It is one of the most important parameters of a combustible mixture. Accurate determination of the laminar flame speed is extremely important for developing and validating chemical kinetic mechanisms [2]. Another important parameter of a combustible mixture is the Markstein length, which characterizes the variation in the local flame speed due to the influence of external stretching and determines the flame instability with respect to preferential diffusion [3,4]. The Markstein length is one of the basic input physicochemical parameters in certain models of premixed turbulent combustion [5]. Therefore, accurate determination of the Markstein length is very important for turbulent combustion modeling.

In the last 50 years, substantial attention has been given to the development of new techniques and the improvement of existing methodologies for experimental determination of the laminar flame speed and Markstein length. Various experimental approaches utilizing different flame configurations, reviewed in Refs. [1,6], have been developed. Currently, due to its simple flame configuration and well-defined flame stretch rate, the constant-pressure spherical flame method [7–19] becomes one of the most favorable methods for measuring the laminar flame speed and Markstein length. In this method, a quiescent homogeneous combustible mixture in a closed chamber is centrally ignited by an electrical spark which results in an outwardly propagating spherical flame. The flame front history, $R_f = R_f(t)$, is recorded by schlieren or shadow photography with a high speed camera. The laminar flame speed and Markstein length are then extracted through different theoretical models (described later).

Recently, a great deal of effort has been devoted to obtaining accurate laminar flame speed and Markstein length utilizing the constant-pressure spherical flame method. For example, the effects of ignition [20,21], radiation [22], non-spherical geometry [23], compression [24], flame instability [25], and non-linear extrapolation [26] have been investigated. However, discrepancies among the laminar flame speeds and Markstein lengths measured by different researchers for the same fuel are still appearing in the literature [27,28] and become a great concern for kinetic mechanism validation. For example, Fig. 1 shows the measured laminar flame speeds, S_u^0, and the Markstein lengths relative to the burned gas, L_b, of methane/air mixtures. Except for the laminar flame speed calculated by PREMIX (solid line) [29], all the experimental results (symbols) were measured using the constant-pressure spherical flame method [7,10,12–14,17–19]. Figure 1a shows that for very lean methane/air mixtures ($\varphi \leqslant 0.7$), there are large discrepancies among the laminar flame speeds measured by different researchers. This is because buoyancy strongly affects the spherical flame

E-mail address: cz@pku.edu.cn

0010-2180/$ - see front matter © 2010 The Combustion Institute. Published by Elsevier Inc. All rights reserved.
doi:10.1016/j.combustflame.2010.09.001

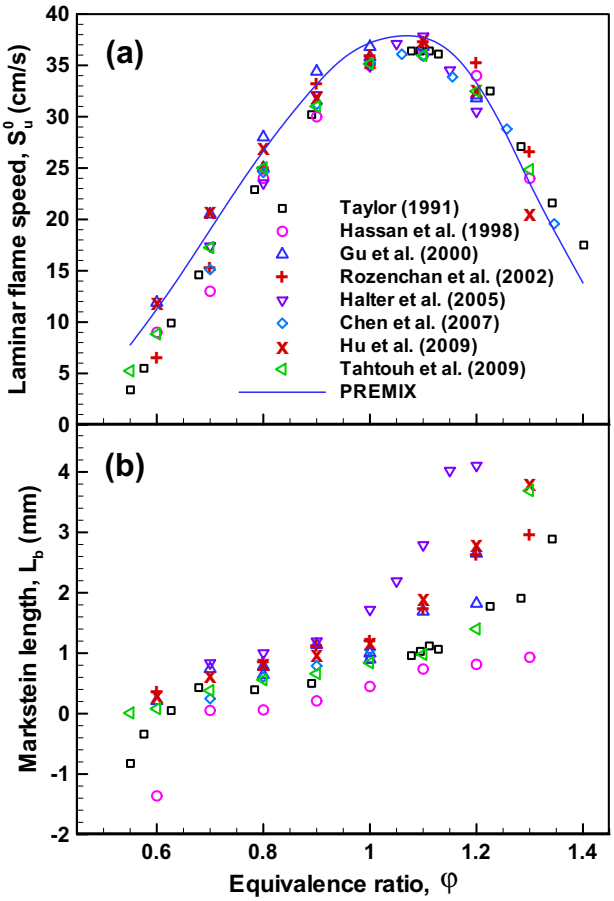

Fig. 1. (a) Laminar flame speed and (b) Markstein length relative to the burned gas for methane/air mixtures at atmospheric pressure and room temperature.

propagation in normal-gravity experiments [16,22]. For near-stoichiometric and rich methane/air mixtures ($\varphi \geqslant 0.8$), the relative difference among the measured laminar flame speeds is shown to be smaller (but still around 10%). Unlike the laminar flame speeds, Fig. 1b shows that there are huge discrepancies for the Markstein lengths measured by different researchers and the relative difference can even be larger than 300%. For example, the Markstein length of rich methane/air mixtures measured by Halter et al. [14] is shown to be several times larger than those by Taylor [7] and Hassan et al. [10]. (The so-called "burned gas Markstein length" shown in Fig. 6 of Ref. [14] is in fact the Markstein length relative to the unburned gas and it is converted to L_b by multiplying the density ratio $\sigma = \rho_b/\rho_u$.)

The reason for these discrepancies has yet to be quantitatively explained. One possible source is the interpretation of the experimental data, particularly for data lying outside of the parameter range over which the assumptions for the theoretical models employed are justified. As an effort to reduce these discrepancies, this study will be focused on the method of extraction. Here "extraction" means to obtain the unstretched laminar flame speed and Markstein length from the spherical flame front propagation history $R_f = R_f(t)$, in the process of which linear extrapolation or linear regression based on a theoretical model (the LM, NM I, or NM II to be introduced below) is conducted. For the constant-pressure spherical flame method, the burned gas is assumed to be quiescent when the pressure rise is negligible [7–19]. As a result, the propagation speed of the experimentally visualized flame front is equal to the flame speed with respect to the burned mixture, i.e. $S_b = dR_f/dt$. For moderate stretch rates, the flame speed can be considered to vary linearly with the stretch rate [4,7,14]

$$S_b = S_b^0 - L_b K, \tag{1}$$

where S_b^0 and L_b are, respectively, the unstretched laminar flame speed and Markstein length with respect to the burned mixture. $K = (2/R_f)dR_f/dt$ is the stretch rate for a propagating spherical flame. Therefore, according to the theoretical model given by Eq. (1), S_b^0 and L_b can be obtained from linear extrapolation based on the plot of S_b versus K [7,14]. Knowing S_b^0, the unstretched laminar flame speed relative to the unburned mixture, S_u^0, can be deduced through mass conservation: $S_u^0 = \sigma S_b^0$, where $\sigma = \rho_b/\rho_u$ is the density ratio.

The linear relation, Eq. (1), linking flame speed to stretch is commonly used to analyze experimental results [7–19]. However, it is not the only model describing propagation spherical flames. Under the assumption of large flame radius, i.e. $R_f \gg 1$, Frankel and Sivashinsky [30] analyzed propagating spherical flames with thermal expansion and the following evolution equation was obtained [30]

$$S_b = S_b^0 - S_b^0 L_b \cdot 2/R_f, \tag{2}$$

which shows that S_b changes linearly with the flame curvature, $2/R_f$. Therefore, S_b^0 and L_b can also be obtained from linear extrapolation based on the plot of S_b versus $2/R_f$. It is noted that historically, Eq. (2) was first proposed by Markstein in 1951 [31].

Unlike these two models given by Eqs. (1) and (2), the following model was used by Kelley and Law [26] in the extraction of S_b^0 and L_b:

$$\ln(S_b) = \ln(S_b^0) - S_b^0 L_b \cdot 2/(R_f S_b), \tag{3}$$

which shows that $\ln(S_b)$ changes linearly with $2/(R_f S_b)$. Consequently, S_b^0 and L_b can also be obtained from linear extrapolation based on the plot of $\ln(S_b)$ versus $2/(R_f S_b)$. Eq. (3) can be obtained from the asymptotic analysis by Ronney and Sivashinsky [32] and Bechtold et al. [33] for propagating spherical flames that are adiabatic and propagate in a quasi-steady manner.

Since the theoretical analysis conducted by Ronney and Sivashinsky [32] and Bechtold et al. [33] was also based on the assumption of large flame radius ($R_f \gg 1$), the model given by Eq. (3) is accurate to the first-order in terms of the inverse of flame radius. As shown in Appendix A, the first two models given by Eqs. (1) and (2) can be readily derived from Eq. (3) in the limit of large flame radius. The error of the LM, NM I, and NM II is shown to be in the same order of $O(1/R_f^2)$. Therefore, Eqs. (1)–(3) can be utilized to extract the laminar flame speed and Markstein length in the constant-pressure spherical flame method. The model given by Eq. (1) shows that the flame speed changes linearly with the stretch rate and thus is referred to as the linear model (LM). Consequently, the other two models given by Eqs. (2) and (3) are referred to as non-linear model I and II (NM I and NM II), respectively. Historically, the LM was used by nearly all the research groups [7–19]; NM I was only discussed by Taylor [7] and was not used by any other researcher; and NM II was only used by Kelley and Law [26] and Halter et al. [42]. Except the recent work conducted by Halter et al. [42], there is no quantitative study investigating the accuracy and performance of these models. In Ref. [42], only the LM and NM II were used to process the experimental data, and the accuracy of these two models was not thoroughly discussed. Therefore, this study will focus on the LM, NM I, and NM II by addressing the following main concerns. First, how accurate are these models in terms of describing propagating spherical flames? Second, what is the performance of these models in extracting the laminar flame speed and Markstein length from propagating spherical flames? Third, which model will give the most accurate laminar flame speed and Markstein length and thus should be used in the propagating spherical flame method?

The paper is organized as follows: in Section 2, theoretical analysis on the accuracy and performance of the LM, NM I, and NM II is

presented; then, in Section 3, numerical simulation is performed to validate the conclusions drawn from theoretical analysis; the performance of the LM, NM I, and NM II in processing the experimental data available in the literature are assessed in Section 4; finally, the conclusions are given in Section 5.

2. Theoretical analysis

Outwardly propagating spherical flames have been analyzed via asymptotic techniques [30,32–35]. However, all these studies [30,32–35] were based on the assumption of large normalized flame radius ($R = R_f/\delta_f^0 \gg 1$, where δ_f^0 is the thickness of an adiabatic planar flame). Consequently, the theoretical results in Refs. [30,32–35] cannot be used to evaluate the accuracy of the LM, NM I, and NM II, all of which are accurate to the first-order in terms of $1/R$ (demonstrated in Appendix A). Only the recent work by He [36] and Chen and Ju [37] spanned all the spherical flame sizes and transitions between flames with small radii (flame kernel after ignition and flame ball) and large radii (propagating spherical flame and planar flame). Therefore, theoretical results of Ref. [37] are utilized here to examine the accuracy and performance of the LM, NM I, and NM II.

There are two main advantages in employing theoretical analysis for the investigation of the LM, NM I, and NM II: (1) the exact values of the laminar flame speed and Markstein length/number are available in the theoretical analysis; they can be compared with the extracted values and thus the accuracy of different extrapolations can be strictly evaluated; and (2) the exact values of the stretched laminar flame speed and stretch rate are available in the theoretical analysis; thus the effects of buoyancy, ignition, non-spherical geometry, radiation, compression, and error from calculating the derivatives can be prevented.

The limitations of the theoretical analysis [37] employed in this study are: thermal expansion is not considered and quasi-steady propagation of the spherical flame front is assumed. To the author's knowledge, all the spherical flame theories in the literature considering the thermal expansion are based on the assumption of large flame radius and thus cannot be used to evaluate the accuracy of the LM, NM I, and NM II due to the reason mentioned before. Nevertheless, detailed numerical simulations considering thermal expansion and unsteady transition are conducted in Section 3 to demonstrate the validity of the theoretical assessment on the accuracy and performance of the LM, NM I, and NM II.

2.1. Different models and their accuracy

For adiabatic, freely propagating spherical flames, we have the following algebraic relationship for flame propagation speed U (normalized by adiabatic planar flame speed, S_u^0) and flame radius R (normalized by adiabatic planar flame thickness, δ_f^0) [37]

$$\frac{e^{UR(1-Le)}}{Le}\frac{\int_R^\infty \tau^{-2}e^{-U\tau}d\tau}{\int_R^\infty \tau^{-2}e^{-ULe\tau}d\tau} = \frac{Z+2\sigma\ln\left(Le^{-1}R^{-2}e^{-URLe}\Big/\int_R^\infty \tau^{-2}e^{-ULe\tau}d\tau\right)}{Z-2\left(1-\sigma\right)\ln\left(Le^{-1}R^{-2}e^{-URLe}\Big/\int_R^\infty \tau^{-2}e^{-ULe\tau}d\tau\right)}, \quad (4)$$

where Le, Z, and σ are, respectively, the Lewis number, the Zel'dovich number, and the ratio of burned to unburned gas densities [37]. The Zel'dovich number is defined as $Z = (1-\sigma)T_a/T_{ad}$, with T_a and T_{ad} being the activation temperature and adiabatic planar flame temperature, respectively [37]. By solving Eq. (4) numerically, we can get the exact solution of flame speed as a function of flame radius [21,37]. Since Eq. (4) is valid for propagating spherical flames with small and large radii, it is referred to as the detailed model (DM) [21]. For flames with large flame radii ($R \gg 1$), the DM reduces to the simplified model (SM) [21]:

$$\left(U+\frac{2}{R}\right)\ln\left(U+\frac{2}{R}\right) = \frac{Z-2}{R}\left(\frac{1}{Le}-1\right). \quad (5)$$

For weakly stretched flames, the stretched flame speed is close to the adiabatic unstretched flame speed (i.e. $U = 1+\varepsilon$ with $|\varepsilon| \ll 1$). In this limit, Eq. (5) reduces to the following models, all accurate to the first-order in terms of $1/R$ (demonstrated by Fig. 3):

$$U = 1 - L^0\cdot 2U/R, \quad U = 1 - L^0\cdot(2/R), \quad \ln(U) = -L^0\cdot 2/(RU), \quad (6a\text{–}c)$$

where $L^0 = Le^{-1} - (Z/2)(Le^{-1}-1)$ is the normalized Markstein length (normalized by the planar flame thickness, δ_f^0), which is the same as that derived for adiabatic premixed counterflow flames [38]. Eqs. (6a–c) are the non-dimensional forms of Eqs. (1)–(3). Therefore, we also refer to these models given by Eqs. (6a–c) as the LM, NM I, and NM II, respectively.

The accuracy of the LM, NM I, and NM II can be assessed by the comparison with the DM. Figure 2 shows the results predicted by the LM, NM I, NM II as well as the DM for $Le = 2.0$, 1.0, and 0.5.

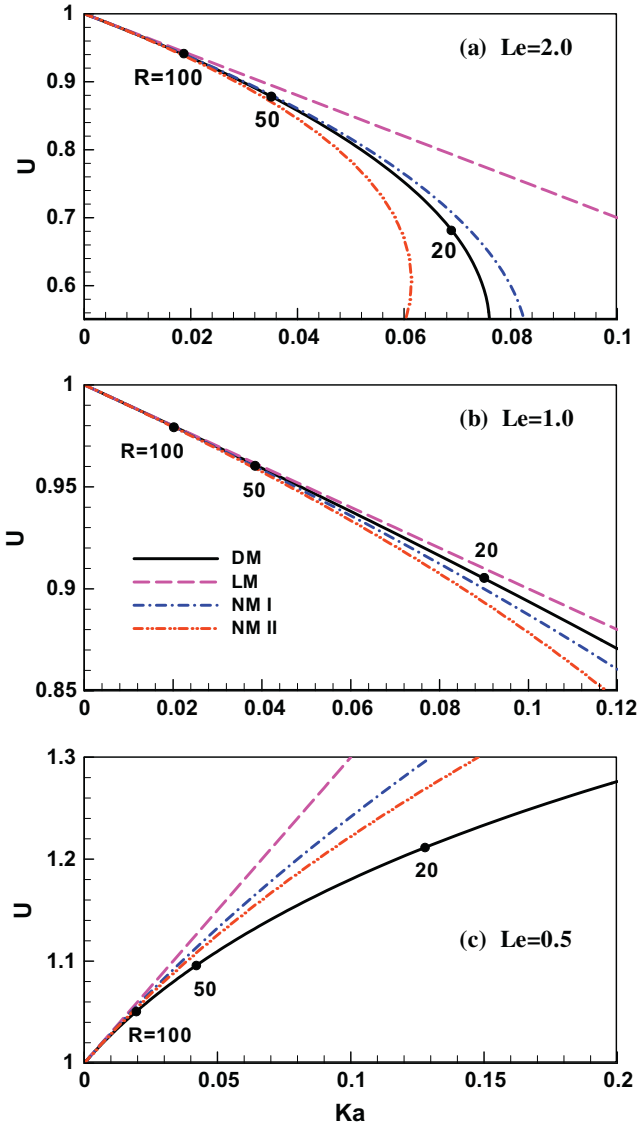

Fig. 2. Flame propagation speed (U) as a function of Karlovitz number ($Ka = 2U/R$) predicted by different models.

It is seen that the predictions by the LM, NM I, and NM II converge to that by the DM when the Karlovitz number ($Ka = 2U/R$) is small enough (or the flame radius is large enough). For large flame radius ($R \geqslant 100$), the results from the LM, NM I, and NM II are shown to be nearly the same as that from the DM. Consequently, the exact unstretched laminar flame speed ($U^0 = 1$) and exact Markstein length ($L^0 = Le^{-1} - (Z/2)(Le^{-1} - 1)$) can be predicted by the LM, NM I, and NM II. For $Le = 1$, the predictions by the LM, NM I, and NM II are shown to be close to that by the DM for the whole range of Karlovitz number considered, while for $Le = 2.0$ and 0.5, there is very large difference between the predictions by the LM, NM I, and NM II and that by the DM, especially for large Karlovitz number. This is because when the Lewis number is appreciably different from unity, the relative difference between the stretched and unstretched flame speeds will be greater than 20% (i.e. $|U - 1| > 0.2$) for large Karlovitz number, as shown in Fig. 2a and c. As a result, the assumption of $|U - 1| = |\varepsilon| \ll 1$ used to derive the LM, NM I, and NM II is not strictly satisfied. According to the DM, the flame speed changes non-linearly with the Karlovitz number for $Le = 2.0$ and $Le = 0.5$. Therefore, as suggested by Kelley and Law [26], non-linear models should be used for mixtures with Lewis numbers appreciably different from unity. Moreover, the accuracy of NM I and NM II are shown to depend on the Lewis number: NM I is closer to the DM than NM II for $Le = 2.0$, while NM II is closer to the DM than NM I for $Le = 0.5$.

To quantitatively show the accuracy of the LM, NM I, and NM II, the error of these models is investigated. According to Eq. (6a–c), the error of the LM, NM I, and NM II is $U - 1 + L^0 \cdot 2U/R$, $U - 1 + L^0 \cdot 2/R$, and $\ln(U) + L^0 \cdot 2/(RU)$, respectively, where R and U are the exact solutions of the DM, and $L^0 = Le^{-1} - (Z/2)(Le^{-1} - 1)$ is the exact Markstein length. The absolute value of the error as a function of R^{-1} is shown in Fig. 3 in a logarithmic scale. The error of all these models is shown to be in the order of R^{-2}. Therefore, the LM, NM I, and NM II are all accurate to the first-order in terms of the inverse of the flame radius. This is consistent with the analysis presented in Appendix A.

In order to assess the accuracy of these models at different Lewis numbers, Fig. 4 shows the error as a function of Lewis number for $R = 50$. Consistent with the results shown in Fig. 2, the error of all these models is shown to increase with the deviation of the Lewis number from a critical value, Le^*, which is slightly less than unity. For $Le < Le^*$, NM II is the most accurate and the LM is the most inaccurate; while for $Le > Le^*$, NM I is the most accurate and the LM is the most inaccurate. Therefore, in order to obtain accurate laminar flame speed and Markstein length for mixtures with different Lewis numbers, different non-linear models should be utilized in the extraction. The LM is shown to be the most inaccurate for mixtures with Lewis number apparently different from unity and can be used only when the Lewis number is close to unity.

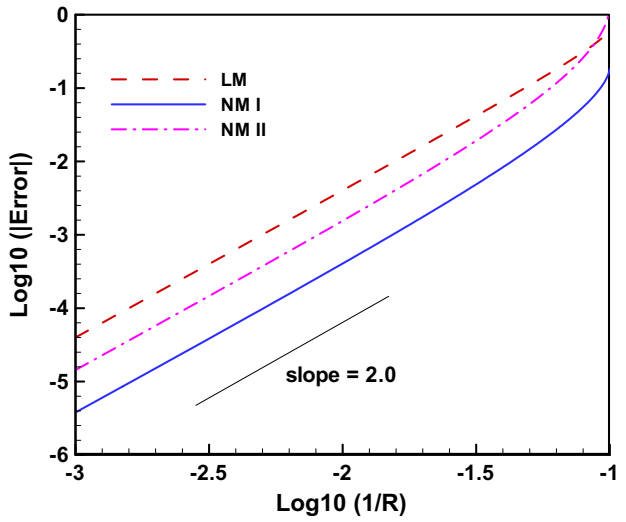

Fig. 3. Error of different models as a function of the inverse of flame radius for $Le = 2.0$.

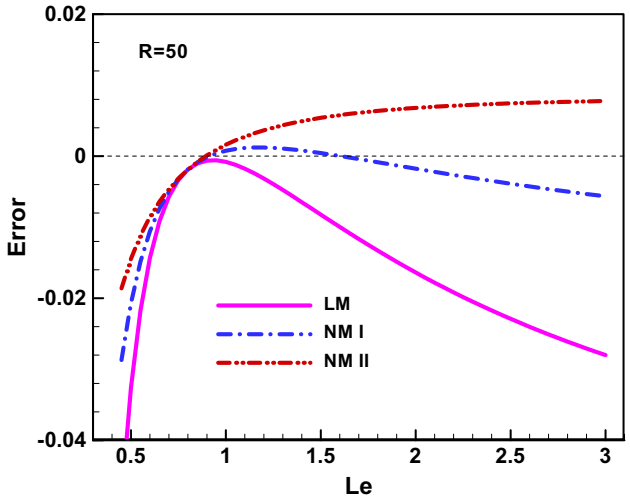

Fig. 4. Error of different models as a function of Lewis number.

2.2. Performance of different models in extraction

In experiments using the constant-pressure spherical flame method [7–19], the laminar flame speed and Markstein length are extracted based on different models using a range of flame radius evolution data, $[R_L, R_U]$. The lower bound, R_L, is chosen to reduce the effects of initial spark ignition and unsteady flame transition on the flame propagation speed [20,21]. The upper bound, R_U, is chosen to ensure that the pressure rise is small (thus the compression effect is negligible [24]) and the flame front is smooth (thus the flame speed is not affected by flame instabilities [25]). To mimic the data processing conducted in spherical flame experiments [7–19], a series of exact solutions, (R, U), from the DM within the range of $R_L \leqslant R \leqslant R_U$ are utilized to extract the laminar flame speed and Markstein length based on different models. The exact values of the laminar flame speed ($U^0 = 1$) and Markstein length ($L^0 = Le^{-1} - (Z/2)(Le^{-1} - 1)$) are available and thus can be used to compare with the extracted results. In this way, the performance of different models can be evaluated. It is noted that the following comparisons are purely mathematical, with no new consideration of the physics (such as radiation, ignition, and compression) that beyond that in Eq. (4).

According to Eqs. (1)–(3) and (6a–c), the formula for extractions based on the LM, NM I, and NM II are respectively

$$U = U^0 - L \cdot 2U/R, \quad U = U^0 - U^0 L \cdot (2/R), \quad \ln(U) = \ln(U^0) - U^0 L \cdot 2/(RU), \tag{7a–c}$$

where U^0 and L are, respectively, the normalized laminar flame speed and Markstein length from extraction.

Figure 5 shows the effects of different models on the extracted laminar flame speed and Markstein length. The extracted and exact unstretched flame speeds, U^0, and Markstein lengths, L, are presented in the tables inset in Fig. 5. For $Le = 1.0$, the relative difference between the extracted values based on different models and the exact values of U^0 and L are within 0.2% and 10%, respectively.

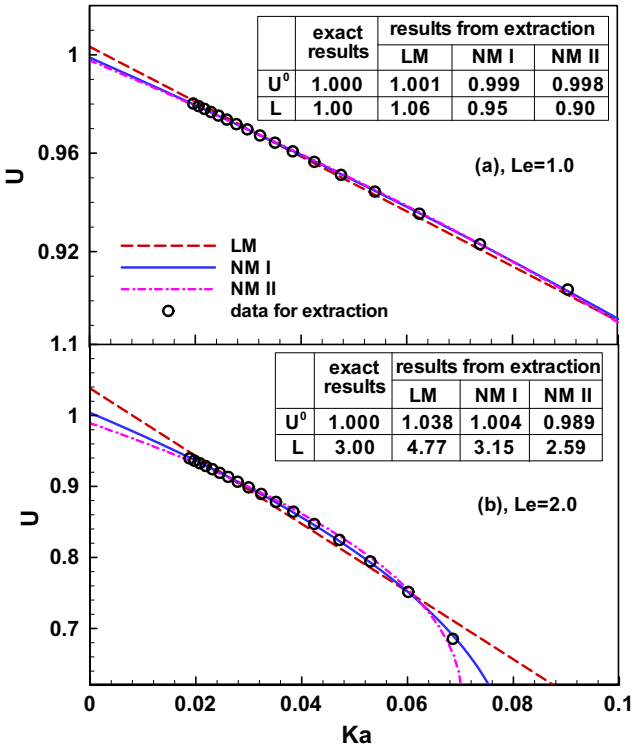

Fig. 5. Effects of different models on the extracted flame speed and Markstein length (the data utilized for extraction are exact results from the DM at $R = 20, 25, \ldots, 100$).

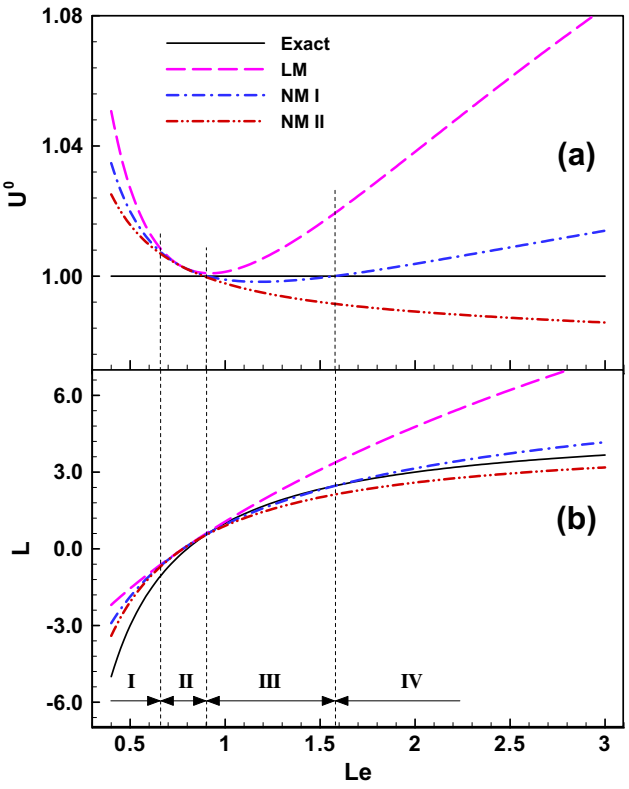

Fig. 6. Extracted (a) flame speeds and (b) Markstein lengths from different models (the data utilized for extraction are exact results from the DM at $R = 20, 25, \ldots, 100$).

Therefore, accurate laminar flame speed and Markstein length can be obtained from extrapolations based on all of these models (the LM, NM I, and NM II). When the Lewis number is appreciably different from unity, $Le = 2.0$, the relative difference between the extracted and exact values of U^0 and L can reach 3.8% and 59%, respectively. Figure 5b shows that both U^0 and L are over-predicted by LM and NM I while they are under-predicted by NM II for $Le = 2.0$. Compared to the exact values of U^0 and L, the results from extraction based on NM I are the most accurate. These results are consistent with the conclusions on the accuracy of different models presented in the previous sub-section.

To assess the performance of different models at different Lewis numbers, Fig. 6 shows the extracted values of U^0 and L from extractions based on LM, NM I, and NM II. The relative difference between extracted and exact values for U^0 is shown to be within 10%, while that for L can reach 200%, which explains why the laminar flame speeds measured by different researchers agree well with one another, while there is a very large discrepancy ($\sim$100%) for the Markstein length (see Fig. 1). The performance of the LM, NM I, and NM II can be compared in four different regimes shown in Fig. 6. In regime I, the extracted results from NM II are the most accurate. In regime II, the extracted results from LM, NM I, and NM II are nearly the same. In regimes III and IV, the extracted results from NM I are the most accurate. Both U^0 and L are slightly under-predicted by NM I in regime III and over-predicted by NM I in regime IV. Therefore, in order to get accurate U^0 and L, non-linear models should be used in the extraction, especially for mixtures with Lewis number appreciably different from unity. Figure 6 shows that NM II should be used for mixtures with small Lewis number (negative Markstein length, regimes I and II) while NM I should be used for mixtures with large Lewis number (positive Markstein length, regimes III and IV).

To quantitatively show the relative difference among the extracted values from different models, the results from the LM (denoted by subscript 'LM') and NM II (denoted by subscript 'NM II') are compared with those from NM I (denoted by subscript 'NM I'). Figure 7 shows that the relative difference increases with $|Le - Le^*|$. Moreover, the relative difference in the Markstein length is shown to be one-order larger that of in the laminar flame speed.

It is noted that the flame radius range used for the extractions shown in Figs. 5–7 is $20 \leqslant R \leqslant 100$. This range is chosen to ensure consistency in the relative difference between the stretched flame speed and unstretched laminar flame speed predicted by theory (Fig. 2), simulations (Figs. 8 and 9), and experiments (Fig. 12). The LM, NM I, and NM II, will certainly give a better accuracy for larger flame radius range than for the smaller range. However, the conclusion on the performance of different models does not change with the flame radius range. This is confirmed by results from extractions based on a larger flame radius range of $50 \leqslant R \leqslant 200$.

Summarizing, the above theoretical analysis basically answers the three questions introduced at the end of Section 1. It is found that the LM, NM I, and NM II can be derived from the DM and are all accurate to the first-order in terms of the inverse of flame radius. The accuracy of the LM, NM I, and NM II is shown to strongly depend on the Lewis number. Therefore, in order to get accurate laminar flame speed and Markstein length from the spherical flame method, different non-linear models should be used for different mixtures.

3. Numerical validation

The theoretical analysis is constrained by the assumptions of constant density (no thermal expansion), constant thermal and transport properties, one-step chemistry, and quasi-steady propagation. Therefore, the comparison based on theoretical results only provides qualitative rather than quantitative information on the

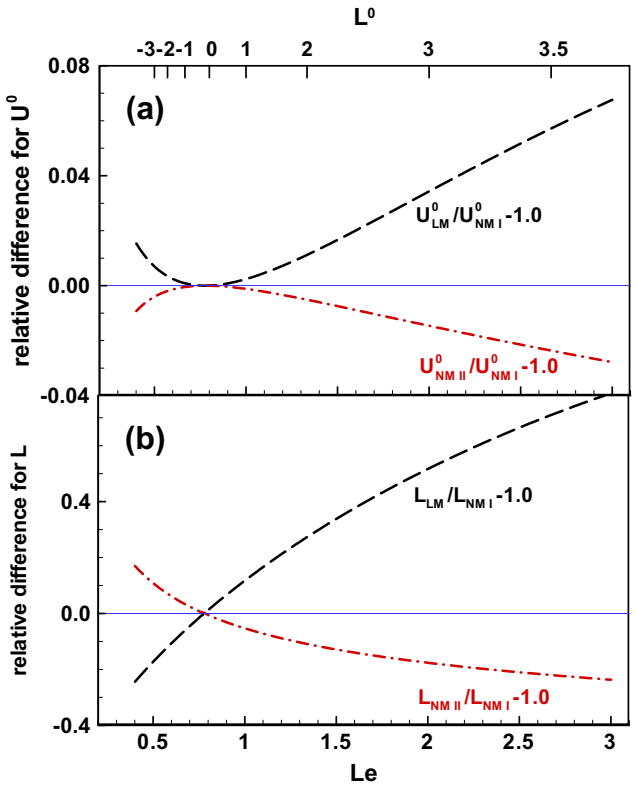

Fig. 7. Relative difference for the extracted (a) flame speed and (b) Markstein length (the data utilized for extraction are exact results from the DM at $R = 20, 25, \ldots, 100$; the exact value of Markstein length is $L^0 = Le^{-1} - (Z/2)(Le^{-1} - 1)$).

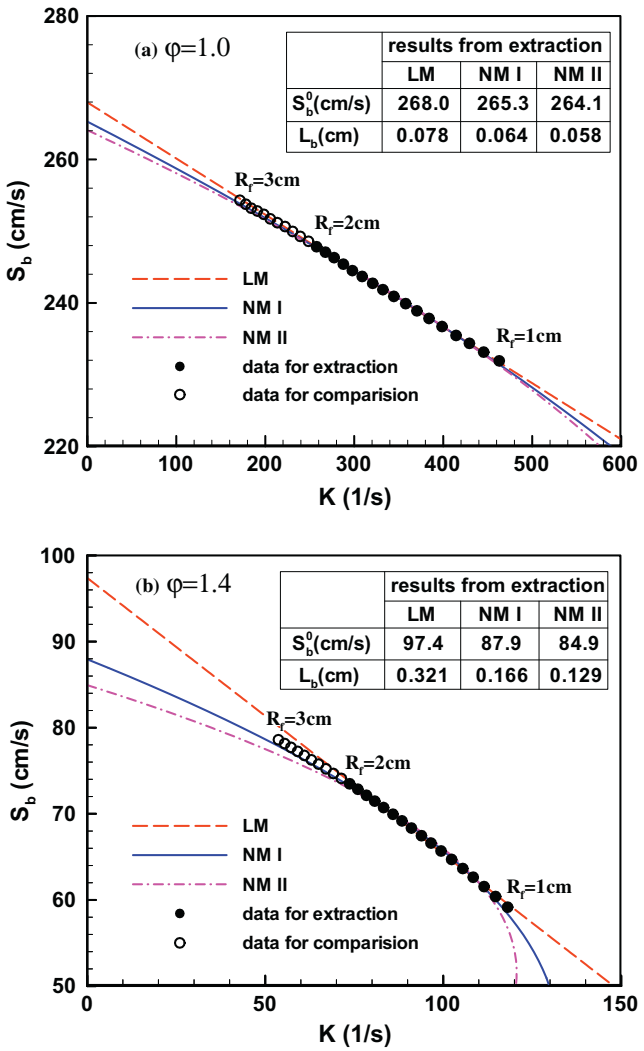

Fig. 8. Effects of different models on the extracted flame speed and Markstein length of methane/air mixtures at atmospheric pressure: (a) $\varphi = 1.0$ and (b) $\varphi = 1.4$.

accuracy and performance of different models. In order to remove these assumptions, detailed numerical simulation of propagating spherical flames is conducted and the validity of the conclusions drawn from theoretical analysis will be demonstrated in the following.

3.1. Numerical methods and specifications

A time-accurate and space-adaptive numerical solver for Adaptive Simulation of Unsteady Reactive Flow, A-SURF (1D), is used to carry out high-fidelity numerical simulation of outwardly propagating spherical flames. A-SURF has been successfully used and validated in a series of studies on spherical flame initiation and propagation [21–24,28,43]. Details on the governing equations, numerical schemes, and code validation of A-SURF can be found in Refs. [21,43] and hence are only briefly described below.

The unsteady compressible Navier–Stokes equations for multicomponent reactive flow are solved in A-SURF [21,43]. The finite volume method is used to discretize the conservation governing equations in the spherical coordinate. The second-order accurate, Strang splitting fractional-step procedure [39] is utilized to separate the time evolution of the stiff reaction term from that of the convection and diffusion terms. In the first fractional step, the non-reactive flow is solved. The Runge–Kutta, MUSCL-Hancock, and central difference schemes, all of second-order accuracy, are employed for the calculation of the temporal integration, convective flux, and diffusive flux, respectively. The chemistry is solved in the second fractional step using the VODE solver [40]. The detailed methane/air reaction mechanism, GRI-MECH 3.0 [41], is used in this study. The chemical reaction rates as well as thermodynamic and transport properties are evaluated using the CHEMKIN and TRANSPORT packages [29] interfaced with A-SURF. To maintain adequate numerical resolution of the moving flame, a multi-level, dynamically adaptive mesh refinement algorithm has been developed and used in A-SURF. Nine grid levels are utilized in this study and grid convergence is tested to ensure the numerical accuracy of the solutions.

In all simulations, the spherical chamber radius is set to be $R_w = 100$ cm (i.e. the computational domain is $0 \leqslant r \leqslant 100$ cm) and only the flame trajectory data with flame radius less than 3.5 cm are utilized for the extraction. As a result, the pressure increase (<0.01%) and compression-induced flow [24] are negligible. The initial and boundary conditions are the same as those in Ref. [43]. The propagating spherical flame is initiated by a small hot pocket (1–2 mm in radius) of burned product surrounded by fresh mixture at room temperature ($T_u = 298$ K) and initially specified pressure. The size of the hot pocket is chosen so that the effects of ignition [20,21] can be minimized. Similar to the theoretical analysis, the effect of radiative loss [22,35,43] is not included in the numerical simulation.

From the flame front history, $R_f = R_f(t)$, defined as the position of maximum heat release in the simulation, $S_b = dR_f/dt$ and $K = (2/R_f)\, dR_f/dt = 2S_b/R_f$ can be calculated from numerical differentiation. Consequently, the unstretched laminar flame speed, S_b^0, and Markstein length, L_b, can be obtained from extractions based on the LM, NM I, and NM II given by Eqs. (1)–(3), respectively.

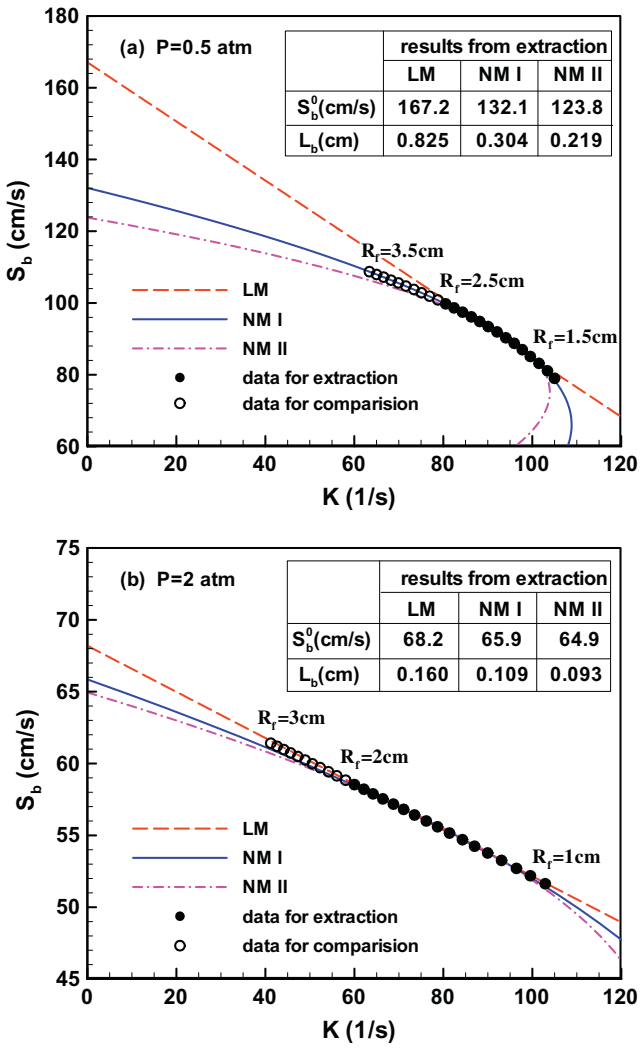

Fig. 9. Effects of different models on the extracted flame speed and Markstein length of rich ($\varphi = 1.4$) methane/air mixture: (a) $P = 0.5$ atm and (b) $P = 2.0$ atm.

3.2. Results and discussions

Figure 8 shows the effects of different models on the extracted laminar flame speed and Markstein length of atmospheric methane/air mixtures at the equivalence ratio of $\varphi = 1.0$ and $\varphi = 1.4$. The flame radius range used for the extraction is $1 \leqslant R_f \leqslant 2$ cm (closed symbols). Flame propagation speed at $2 \leqslant R_f \leqslant 3$ cm (from the same simulation, denoted by open symbols) is shown to elucidate the performance of different extrapolation methods. For $\varphi = 1.0$, the Markstein length is less than 1 mm and the Lewis number is close to unity [38]. Figure 8a shows that the LM, NM I, and NM II give very close results: the maximum relative differences among the extracted values for S_b^0 and L_b are 1.5% and 34.5%, respectively. This is similar to the theoretical results for $Le = 1.0$ shown in Fig. 5a. With the increase of the equivalence ratio, the Markstein length and Lewis number of methane/air mixtures increase [38]. For $\varphi = 1.4$, Fig. 8b shows that the stretched flame speed, S_b, changes non-linearly with the stretch rate, K, and the maximum relative differences among the extracted values from different models for S_b^0 and L_b are 14.7% and 149%, respectively. Figure 8b also shows that NM I fits the data for comparison much better than the LM and NM II. Therefore, the extracted results from NM I are the most accurate, while those from LM and NM II are over-predicted and under-predicted, respectively. Again, this is similar to the theoretical results for $Le = 2.0$ shown in Fig. 5b.

The Markstein length is known to be strongly affected by pressure [38]. To further assess the performance of different models for mixtures with different Markstein lengths, Fig. 9 shows the results for rich ($\varphi = 1.4$) methane/air mixture at $P = 0.5$ atm and $P = 2.0$ atm. The Markstein length at 0.5 atm is much larger than that at 2.0 atm. As a result, Fig. 9 shows that the difference among the extracted results increases with the decrease of pressure (i.e. increase of the Markstein length). This is consistent with the theoretical results in Fig. 7 which shows the relative difference increases with the Markstein length. Furthermore, Fig. 9a shows that NM I almost exactly fits the data for comparison and thus NM I are much more accurate than the LM and NM II. Compared to the results extracted from NM I, the over-predictions in S_b^0 and L_b by the LM are 26.6% and 171.4%, respectively, and the under-predictions in S_b^0 and L_b by NM II are 6.3% and 28.0%, respectively.

Figure 10 shows the extracted results from three different models for atmospheric methane/air mixtures at different equivalence ratios. For each equivalence ratio, the Markstein length is shown to be positive and thus the corresponding Lewis number, Le, is larger than the critical value, Le^*, which is slightly less than unity [38]. Figure 10 shows that the extracted values of S_b^0 and L_b from NM I are always smaller than those from the LM while larger than those from NM II. This is consistent with the theoretical results that the LM gives the largest extracted values (for both laminar flame speed and Markstein length) while NM II gives the smallest extracted values (see Fig. 6). According to the theoretical analysis, when $Le > Le^*$ (positive Markstein length), the laminar flame speed and Markstein length are both over-predicted (under-predicted) by the LM (NM II) and NM I is the most accurate. Therefore, for methane/air mixtures, NM I should be used in the extraction. Otherwise, as shown by Figs. 10b and 1b, the Markstein length of very rich methane/air mixtures will be significantly over-predicted (~100%) by extractions based on the LM.

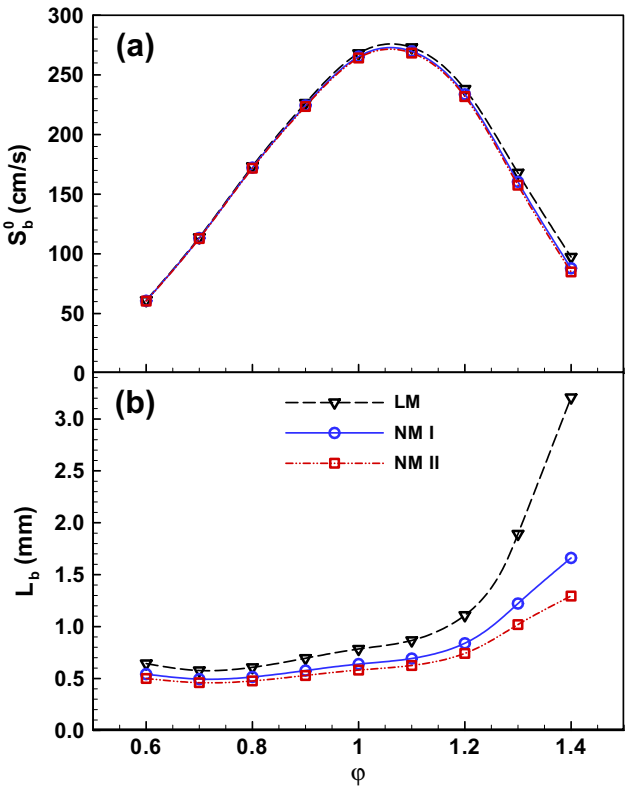

Fig. 10. Extracted (a) flame speed and (b) Markstein length of methane/air mixtures from different models (the data in the flame radius range of $1 \leqslant Rf \leqslant 2$ cm are utilized for extraction).

Figure 11 shows the relative differences among S_b^0 and L_b extracted from different models. It is noted that the Lewis number or the Markstein length can be easily changed in the theoretical analysis while this change is realized by varying the equivalence ratio of methane/air mixtures in the numerical simulation. The magnitude of the relative differences is shown to increase monotonically with the equivalence ratio. This is due to the similar monotonic change of the Markstein length (or the Lewis number) with the equivalence ratio shown in Fig. 10b. Therefore, the simulation results shown in Fig. 11 are consistent with the theoretical predictions shown in Fig. 7: the relative differences for U^0 and L both increase with the Markstein length (or the Lewis number) when $L^0 > 0$ (or $Le > Le^*$). Furthermore, comparison between Fig. 11a and b shows that the relative difference for the Markstein lengths predicted by different models is about one-order larger than that for the laminar flame speeds. As a result, the extracted value of the Markstein length depends on theoretical models much more strongly than that of the laminar flame speed. The same conclusion is also drawn from theoretical results shown in Fig. 7.

Summarizing, similar conclusions to those from theoretical analysis are drawn from numerical simulations including thermal expansion and detailed kinetic and transport properties. The effects of different models are found to increase with the magnitude of the Markstein length (or $|Le - Le^*|$) and the extracted values of S_b^0 and L_b from NM I are always smaller than those from the LM while larger than those from NM II. Moreover, NM I is shown to be the most accurate for CH_4/air mixtures for which the Markstein length is positive.

4. Application in processing experimental data

In this section, the LM, NM I, and NM II are utilized to process the experimental data available in the literature and to further validate the theoretical results in Section 2. Many studies (see, for example, Refs. [7–19]) reported the unstretched laminar flame speeds and Markstein lengths measured from spherical flame experiments. However, only a few of them reported the stretched flame speed as a function of flame radius or stretch rate, which can be utilized to test the performance of the LM, NM I, and NM II. In this study, the experimental data for methane/air from Figs. 20 and 21 of Ref. [7] are used.

Figures 12–14 show the results for methane/air mixtures from extractions based on experimental data reported by Taylor [7]. The effects of different models on the extracted flame speed and Markstein length of methane/air with $\varphi = 1.0$ and $\varphi = 1.34$ (the corresponding stoichiometry used in Ref. [7] is 1.0 and 1.3, respectively) are shown in Fig. 12. Similar to the numerical results shown in Fig. 8, it is seen that with the increase of the equivalence ratio, the Markstein length (or the Lewis number) increases and so does the difference among the extracted results from different models. For $\varphi = 1.0$, Fig. 12a shows that LM, NM I, and NM II give very close results: the maximum relative differences among the extracted values for S_b^0 and L_b are 2.2% and 46.8%, respectively. This is similar to the theoretical results for $Le = 1.0$ shown in Fig. 5a. Moreover, the extracted values of S_b^0 and L_b are found to be very close to the numerical results shown in Fig. 8a. For $\varphi = 1.34$, the stretched

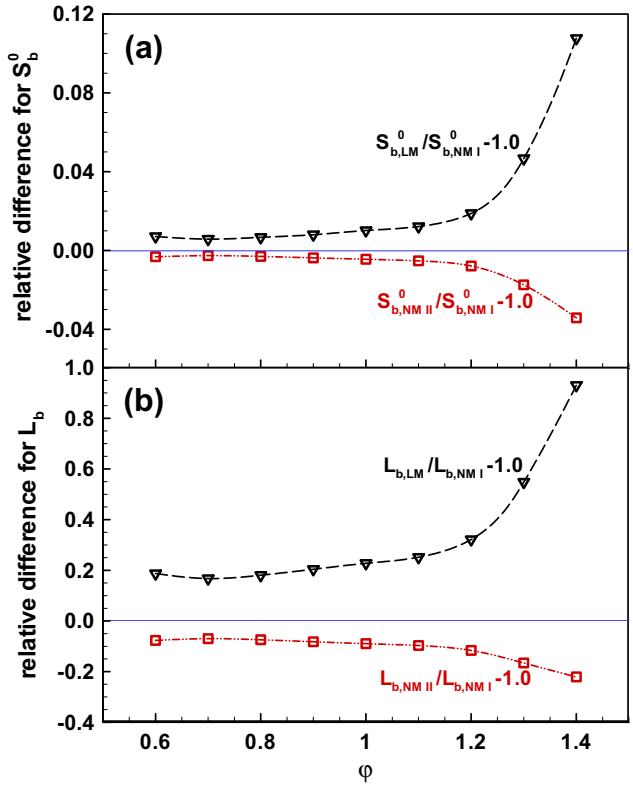

Fig. 11. Relative difference for the extracted (a) flame speed and (b) Markstein length of methane/air mixtures (the data in the flame radius range of $1 \leqslant R_f \leqslant 2$ cm are utilized for extraction).

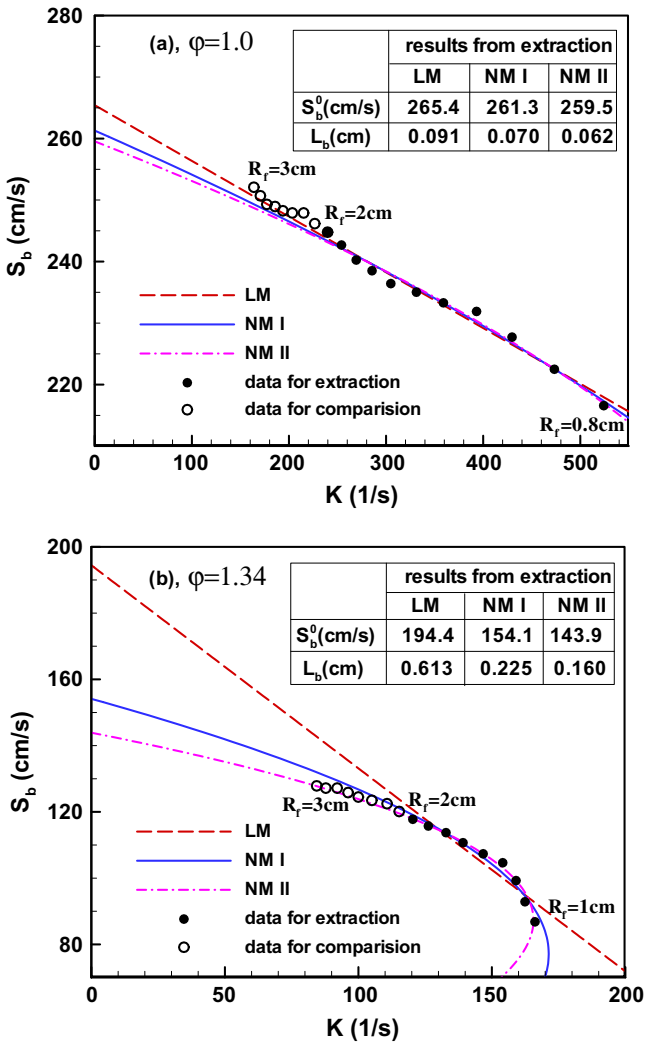

Fig. 12. Effects of different models on the extracted flame speed and Markstein length of methane/air mixtures: (a) $\varphi = 1.0$ and (b) $\varphi = 1.34$ (the data utilized for extraction and comparison are from experiments conducted by Taylor [7]).

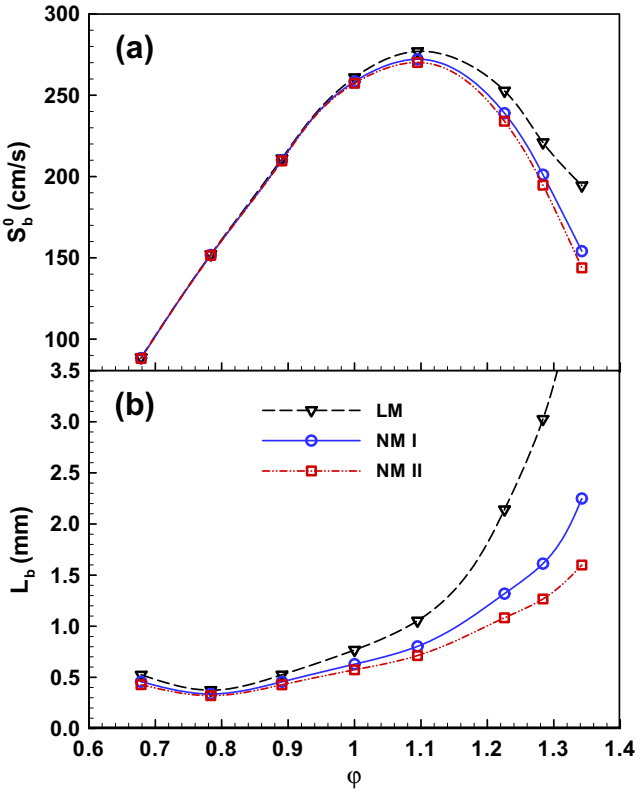

Fig. 13. Extracted (a) flame speed and (b) Markstein length of methane/air mixtures from different models (the data in the flame radius range of $1 \leqslant R_f \leqslant 2$ cm utilized for extraction are from experiments conducted by Taylor [7]).

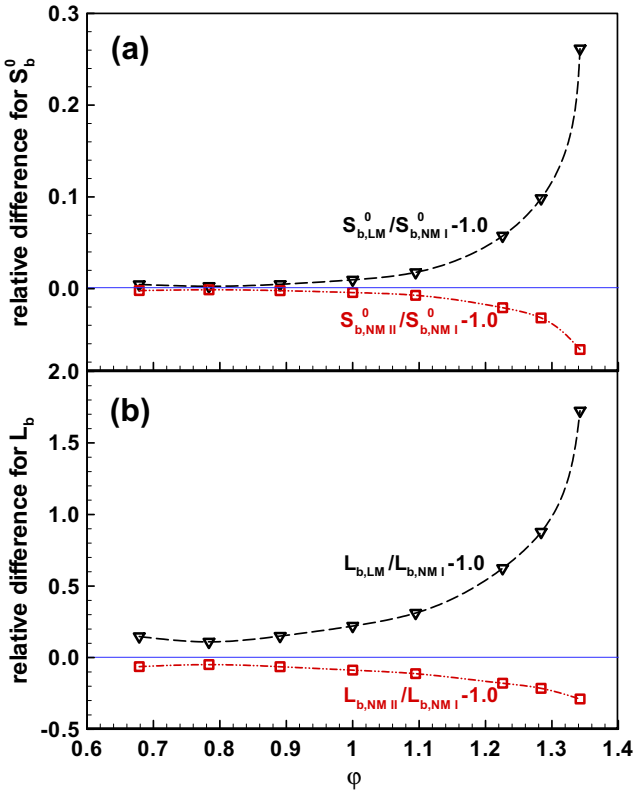

Fig. 14. Relative difference for the extracted (a) flame speed and (b) Markstein length of methane/air mixtures (the data in the flame radius range of $1 \leqslant R_f \leqslant 2$ cm utilized for extraction are from experiments conducted by Taylor [7]).

flame speed, S_b, is shown to change non-linearly with the stretch rate, K, and the maximum relative differences among the extracted values from different models for S_b^0 and L_b are 35.1% and 283.1%, respectively. According to the theoretical analysis, NM I is the most accurate since the Markstein length is positive and the extracted results from the LM and NM II are over-predicted and under-predicted, respectively. The extractions above are based on data with flame radius less than 2 cm. Similar to numerical results in Fig. 8, Fig. 12 also shows the experimental results for flame propagation speed at $2 \leqslant R_f \leqslant 3$ cm (denoted by open symbols). However, we cannot judge which model is the most accurate by simply comparing the results predicted by models (lines) and those measured in experiments (open symbols in Fig. 12). This is because, unlike the simulation results, the experimental data at large flame radii might be affected by radiation [22], compression [24], and flame instabilities [25]. Consequently, these effects will be reflected in the extracted flame speed and Markstein length, even if the appropriate model is used.

Figures 13 and 14 show the extracted results and relative differences as functions of equivalence ratio. These results are similar to the simulation results presented in Figs. 10 and 11. Besides, the performance of the LM and NM II was also compared in Ref. [42] and similar results to those in Fig. 13 were reported (see Figs. 4 and 5 of Ref. [42]). Therefore, the conclusions on the performance of the LM, NM I, and NM II drawn from theoretical analysis are also confirmed via processing experimental data of propagating spherical flames. As mentioned before, the Markstein length is positive for methane/air mixtures with $0.6 \leqslant \varphi \leqslant 1.4$ and thus we have $Le > Le^*$. Consistent with the theoretical results shown in Figs. 6 and 7, Figs. 13 and 14 show that the flame speed and Markstein length are both over-predicted (under-predicted) by the LM (NM II) compared to those by NM I. It is seen that if the LM is used to process the experimental data for rich methane/air mixtures, the over-prediction of laminar flame speed is in the order of 10% while that of Markstein length is in the order of 100%. The relative difference from experiments (Fig. 14) is shown to be about two times that from simulation (Fig. 11). This is because there is much larger scatter in the experimental results [7] than that in the simulation.

5. Conclusions

One linear model (LM) and two non-linear models (NM I and NM II) utilized for extracting the laminar flame speed and Markstein length in the constant-pressure spherical flame method are studied theoretically and numerically. The detailed model (DM) valid for propagating spherical flames with small and large radii is presented first. The LM, NM I, and NM II are then derived from the DM. It is shown that the LM, NM I, and NM II are all accurate to the first-order in terms of the inverse of flame radius and thus can be utilized to extract the laminar flame speed and Markstein length in the constant-pressure spherical flame method.

The accuracy of the LM, NM I, and NM II is found to strongly depend on the Lewis number. It is demonstrated that NM I is the most accurate for mixtures with large Lewis number (positive Markstein length) while NM II is the most accurate for mixtures with small Lewis number (negative Markstein length). Therefore, in order to get accurate laminar flame speed and Markstein length from the spherical flame method, different non-linear models should be used for different mixtures. For mixtures with Lewis number appreciably different from unity, both the laminar flame speed and the Markstein length are over-predicted from extractions based on the LM. The over-prediction by the LM for laminar flame speed is within 10%, while that for Markstein length can reach 100% or even larger. The above conclusions drawn from

theoretical analysis are confirmed by conducting detailed numerical simulation and processing experimental data available in the literature.

Acknowledgments

This work was supported by National Natural Science Foundation of China (Grant No. 50976003). Mr. Zhenlong Zhao at Peking University is thanked for his help on processing the experimental data available in the literature. Prof. Yiguang Ju and Mr. Michael P. Burke at Princeton University are thanked for helpful discussions. The referees are thanked for providing constructive comments and help in improving the paper.

Appendix A

The theoretical analysis conducted by Ronney and Sivashinsky [32] and Bechtold et al. [33] was based on the assumption of large flame radius ($R_f \gg 1$). Therefore, Eq. (3) can be exactly written as

$$\left(\frac{S_b}{S_b^0}\right)\ln\left(\frac{S_b}{S_b^0}\right) = -\frac{2L_b}{R_f} + O\left(\frac{1}{R_f^2}\right), \tag{A1}$$

in which the second term on the right hand side represents the error in the order of $\left(1/R_f^2\right)$. In the limit of large flame radius (or moderate stretch rate), the normalized flame propagation speed, S_b/S_b^0, can be written in the following asymptotic form:

$$\frac{S_b}{S_b^0} = 1 + \varepsilon + O\left(\frac{1}{R_f^2}\right) \text{ with } \varepsilon \sim \frac{1}{R_f}. \tag{A2}$$

Substituting Eq. (A2) into (A1) and using $\ln(1+x) = x - x^2 + O(x^3)$ for $x \ll 1$, we get

$$\varepsilon = -2L_b/R_f. \tag{A3}$$

Therefore, according to Eqs. (A2) and (A3), we have the exact form of NM I as

$$\frac{S_b}{S_b^0} = 1 - \frac{2L_b}{R_f} + O\left(\frac{1}{R_f^2}\right). \tag{A4}$$

According to the definition of the stretch rate, we have

$$\frac{K}{S_b^0} = \frac{2}{R_f}\frac{S_b}{S_b^0} = \frac{2}{R_f}\left[1 - \frac{2L_b}{R_f} + O\left(\frac{1}{R_f^2}\right)\right] = \frac{2}{R_f} + O\left(\frac{1}{R_f^2}\right), \tag{A5}$$

in the derivation of which Eq. (A4) is used. Substituting Eq. (A5) in (A4), we get the exact form of the LM as

$$\frac{S_b}{S_b^0} = 1 - \frac{L_b}{S_b^0}K + O\left(\frac{1}{R_f^2}\right). \tag{A6}$$

Therefore, according to Eqs. (A6), (A4), and (A1), the error of the LM, NM I, and NM II given by Eqs. (1)–(3) is in the same order of $O(1/R_f^2)$.

References

[1] G.E. Andrews, D. Bradley, Combust. Flame 18 (1972) 133–153.
[2] C.K. Law, C.J. Sung, H. Wang, T.F. Lu, AIAA J. 41 (2003) 1629–1646.
[3] G.H. Markstein, Nonsteady Flame Propagation, Pergamon Press, 1964.
[4] P. Clavin, Prog. Energy Combust. Sci. 11 (1985) 1–59.
[5] N. Peters, Turbulent Combustion, Cambridge University Press, New York, 2000.
[6] C.J. Rallis, A.M. Garforth, Prog. Energy Combust. Sci. 6 (1980) 303–329.
[7] S.C. Taylor, Burning Velocity and the Influence of Flame Stretch, Ph.D. Thesis, University of Leeds, 1991.
[8] L.K. Tseng, M.A. Ismail, G.M. Faeth, Combust. Flame 95 (1993) 410–426.
[9] D. Bradley, R.A. Hicks, M. Lawes, C.G.W. Sheppard, R. Woolley, Combust. Flame 115 (1998) 126–144.
[10] M.I. Hassan, K.T. Aung, G.M. Faeth, Combust. Flame 115 (1998) 539–550.
[11] S.D. Tse, D.L. Zhu, C.K. Law, Proc. Combust. Inst. 28 (2000) 1793–1800.
[12] X.J. Gu, M.Z. Haq, M. Lawes, R. Woolley, Combust. Flame 121 (2000) 41–58.
[13] G. Rozenchan, D.L. Zhu, C.K. Law, S.D. Tse, Proc. Combust. Inst. 29 (2003) 1461–1470.
[14] F. Halter, C. Chauveau, N. Djeballi-Chaumeix, I. Gokalp, Proc. Combust. Inst. 30 (2005) 201–208.
[15] Z. Huang, Y. Zhang, K. Zeng, B. Liu, Q. Wang, D.M. Jiang, Combust. Flame 146 (2006) 302–311.
[16] L. Qiao, Y. Gu, W.J.A. Dam, E.S. Oran, G.M. Faeth, Combust. Flame 151 (2007) 196–208.
[17] Z. Chen, X. Qin, Y.G. Ju, Z.W. Zhao, M. Chaos, F.L. Dryer, Proc. Combust. Inst. 31 (2007) 1215–1222.
[18] E. Hu, Z. Huang, J. He, C. Jin, J. Zheng, Int. J. Hydrogen Energy 34 (2009) 4876–4888.
[19] T. Tahtouh, F. Halter, C. Mounaïm-Rousselle, Combust. Flame 156 (2009) 1735–1743.
[20] D. Bradley, P.H. Gaskell, X.J. Gu, Combust. Flame 104 (1996) 176–198.
[21] Z. Chen, M.P. Burke, Y. Ju, Proc. Combust. Inst. 32 (2009) 1253–1260.
[22] Z. Chen, X. Qin, B. Xu, Y.G. Ju, F.S. Liu, Proc. Combust. Inst. 31 (2007) 2693–2700.
[23] M.P. Burke, Z. Chen, Y. Ju, F.L. Dryer, Combust. Flame 156 (2009) 771–779.
[24] Z. Chen, M.P. Burke, Y. Ju, Combust. Theory Modell. 13 (2009) 343–364.
[25] D. Bradley, M. Lawes, K. Liu, S. Verhelst, R. Woolley, Combust. Flame 149 (2007) 162–172.
[26] A.P. Kelley, C.K. Law, Combust. Flame 156 (2009) 1006–1013.
[27] J.T. Farrell, R.J. Johnston, I.P. Androulakis, SAE Paper, 2004-01-2936.
[28] Z. Chen, Int. J. Hydrogen Energy 34 (2009) 6558–6567.
[29] R.J. Kee, J.F. Grcar, M.D. Smooke, J.A. Miller, Sandia National Laboratory Report SAND85-8240, 1985.
[30] M.L. Frankel, G.I. Sivashinsky, Combust. Sci. Technol. 31 (1983) 131–138.
[31] G.H. Markstein, J. Aeronaut. Sci. 18 (1951) 199–209.
[32] P.D. Ronney, G.I. Sivashinsky, SIAM J. Appl. Math. 49 (1989) 1029–1046.
[33] J.K. Bechtold, C. Cui, M. Matalon, Proc. Combust. Inst. 30 (2005) 177–184.
[34] J.K. Bechtold, M. Matalon, Combust. Flame 67 (1987) 77–90.
[35] Z. Chen, X. Gou, Y. Ju, Combust. Sci. Technol. 182 (2010) 124–142.
[36] L. He, Combust. Theory Modell. 4 (2000) 159–172.
[37] Z. Chen, Y. Ju, Combust. Theory Modell. 11 (2007) 427–453.
[38] C.K. Law, Combustion Physics, Cambridge University Press, 2006.
[39] G. Strang, SIAM J. Numer. Anal. 5 (1968) 506–517.
[40] P.N. Brown, G.D. Byrne, A.C. Hindmarsh, SIAM J. Sci. Stat. Comput. 10 (1989) 1038–1051.
[41] G.P. Smith et al. <http://www.me.berkeley.edu/gri_mech/>.
[42] F. Halter, T. Tahtouh, C. Mounaïm-Rousselle, Combust. Flame 157 (2010) 1825–1832.
[43] Z. Chen, Combust. Flame (2010), doi:10.1016/j.combustflame.2010.07.010.